3
Utilization of Multicomponent 2D Quasicrystal Nanosheets for NO_2 Sensor

This chapter 3, we investigate the detailed synthesis process of metallic multicomponent two-dimensional quasicrystal nanosheets. This is followed by a detailed description of the materials and electrical properties. 2D quasicrystal nanosheets provide an effective sensitive response for sensing due to the large surface area available for the analyte. $Al_{70}Co_{10}Fe_5Ni_{10}Cu_5$ (Quasicrystal-QC) alloy can be effectively exfoliated into a 2D form consisting of the decagonal quasicrystalline phase. The ultrathin thickness of a few nm (~6 nm) was achieved, exhibiting anisotropic electron-transport properties. The 2D-QC shows pseudo-conducting behavior in the planar region, which endowed the material in nanosheets to work as ultrasensitive NO_2 gas sensors (1-100 ppm) at 100°C. The fabricated device exhibits a NO_2 gas response ($\Delta R/R_a$ %) of 46% (100 ppm NO_2) compared to its bulk counterpart its response is 3 times larger. In addition, the mechanism of gas sensing was further corroborated using density functional theory (DFT) simulations and strongly supported the interpretation of the experimental data.

3.1 INTRODUCTION

2D materials can exhibit ultrasensitive responses due to the quantum confinement of electrons and high specific surface area to be functionalized and used as a platform to enhance their responses for sensing, catalysis, energy storage, optoelectronic devices, and biomedicine application *(Rodin et al., 2020)*, *(X. Liu & Hersam, 2018; Yao et al., 2019)* etc. Despite the availability and wide-scale investigation of well-known 2D materials, like graphene, transition metal dichalcogenides (TMDCs), metal carbide/nitride, Mxenes *(Anasori et al., 2017; Chae et al., 2019)* etc., multicomponent alloys also attracted the attention of the researchers for the various functional applications due to their tunable properties in ample compositional space and varied surface microstructures *(Katiyar et al., 2021a; Kumar Katiyar et al., 2021)*, which are capable of addressing many of the important issues in sensing and catalytic activity. Multi-component alloys (including 2D Quasicrystals) are unique due to their atomic mixing (five or more metal elements in equiatomic or near equiatomic composition with each element contribution ≥5 and ≤ 35 atoms %) and their simple crystal structure. As an example, it is worth mentioning that 2D MoS_2-decorated with FCC multi-component (Ag-Au-Cu-Pd-Pt) nanoparticles exhibited enhanced (ten times) response to H_2 gas sensing (Urs et al., 2020). Multi-element alloys have been receiving increased attention as catalytic materials due to their unique electronic properties and surface chemistry having noble elements or low-cost transition elements (Nellaiappan et al., 2020a). The multicomponent metallic alloy phases with Face Centred Cubic (FCC), Body Centred Cubic (BCC), and hexagonal closed packing (HCP) crystal structures have been reported to exhibit metallic characteristics, but quasi-crystalline ones are anisotropic for electron transport characteristics. The metallic materials exhibiting quasicrystalline structures have long-range aperiodic arrangements, resulting in weak interlayer bonding, which can be exfoliated into 2D layers of quasicrystalline phases with metallic elements, e.g., (Al-Pd-Mn), (Al-Cu-Co), (Al-Co-Ni), etc *(Yadav et al., 2018)*.

On the other hand, multi-principal element mxenes or high entropy metal alloy/carbides, $M_4C_3T_x$ ($TiVNbMoC_3T_x$and $TiVCrMoC_3T_x$) were also reported to be made into 2D layers *(Jishnu et al., 2022a; Nemani et al., 2021)*. These extensive studies reveal that although the bulk (3D) and nanocrystalline multicomponent alloy nanoparticles (0D) have been widely studied, detailed investigations on the synthesis and sensing properties of the 2D multicomponent alloy are yet to

be reported. Under the electronic transport property, by their intrinsic topological properties, quasicrystals unusually exhibit anisotropic electronic properties *(Dolinšek et al., 2012)*. For example, along one crystallographic direction, it can behave like a conductor, while in another one, it can act as an insulator. Therefore, these unique properties due to quasiperiodic materials can be effectively exploited for functional applications. Newly reported 2D nanomaterials have emerged as good candidates to develop novel sensors with enhanced sensitivity as well as selectivity *(D. Tyagi et al., 2020)*.

Here, we reported the synthesis of 2D Quasicrystalline (metallic) from multicomponent alloy $Al_{70}Co_{10}Fe_5Ni_{10}Cu_5$. It is the first time that this kind of nanosheet is obtained using exfoliation methods and then integrated with a gas sensor to detect gas at low temperatures with a cost advantage over other gas sensors (Xuan et al., 2020). The designed sensor exhibits high selectivity and sensitivity toward NO_2 gas at relatively low temperatures *(K. Xu et al., 2022)*. The activity of the 2D QC or conductivity anisotropy was also investigated using DFT simulations, and the results were used to validate the experimental data.

3.2 EXPERIMENTAL

3.2.1 Synthesis of bulk and exfoliated $Al_{70}Co_{10}Fe_5Ni_{10}Cu_5$

The polycrystalline alloy was produced from high-purity elements; Al (purity 99.95%, Alfa Aesar), Co (purity 99.90%, Alfa Aesar), Fe (purity 99.99%, Alfa Aesar), Ni (purity 99.5%, Alfa Aesar), and Cu (purity 99.5%, Sigma Aldrich) via arc melting method. The constituents were mixed and melted five times to ensure homogeneity, according to their nominal composition $Al_{70}Co_{10}Fe_5Ni_{10}Cu_5$. Because of its oxygen-absorbing properties, the chamber was purified before the alloy melted by melting a Ti button. Before annealing, the button ingot was sealed in a quartz tube containing an inert Ar and then kept in the furnace for 48 h at 1000°C. Due to its highly brittle nature, the ingot could be easily crushed to a fine powder. The isopropyl alcohol (IPA) was used as a dispersant to obtain the atomically thin alloy sheets, and the bulk sample was sonicated in a pressurized ultrasound reactor. For the solvent-assisted chemical exfoliation, a small amount (40 mg) of hand-crushed QC powder was suspended in 500 ml of IPA and sonicated for 4h. The liquid phase exfoliation was induced by the high-amplitude sonication waves exerting high shear forces on the surface of the bulk material.

3.2.2 Characterization

The X-ray diffraction (XRD, PANalytical Empyrean diffractometer operating at 35mA, 40kV) was used to determine the phases of the pre and post-exfoliated samples. A scanning electron microscope (SEM, Nova NanoSEM 450 at an acceleration voltage of 15 kV) was used to investigate the surface morphology, and the chemical composition was estimated by an energy-dispersive X-ray spectroscope (EDS) equipped with SEM. The thickness of the exfoliation-produced nanosheet was analyzed by the atomic force microscope (AFM, Asylum research). FEI Titan FEG high-resolution transmission electron microscope (HRTEM) operating at 300 kV was used to explore the microstructural details of the samples. The absorption spectra of the samples were recorded using a dual-beam spectrophotometer (Thermo Scientific, Evolution 201).

3.2.3 Fabrication of NO_2 sensing device

An equal quantity (1 mg) of bulk quasicrystal and 2D Quasicrystal nanosheet suspension in 1 ml ethanol, was prepared by ultrasonication for 6 hours. The resistive gas sensor device was fabricated after depositing an interdigital electrode (IDE) of Cr/Au (20 nm/ 200 nm) on the SiO_2 substrate by a thermal evaporation system using a shadow mask. The prepared suspension was drop-cast by micropipette on fabricated SiO_2 devices with the same concentration (30 µl) on each

device for bulk and 2D-quasicrystal sensor. After drop-casting, the fabricated device was annealed in a furnace at 150 °C for 20 min in an N_2 atmosphere to improve the adhesion.
NO_2 sensing characteristics of the sensors were carried out by using a Keithley semiconductor characterization system source meter 2636B. Gas-sensing characteristics of sensors were evaluated for various NO_2 gas concentrations (1−100 ppm) at a temperature of 100 °C. We have studied the temperature-dependent gas-sensing performance of sensors at fixed NO_2 concentrations to 100 ppm. To further study, the gas sensor's selectivity and device response was studied in the presence of 100 ppm NO_2, NH_3, H_2S, H_2, and SO_2 at 100 ppm. We would like to stress that as in a strongly acidic or basic environment, metals react to form salt and release H_2, our sensor devices were not designed to work in such environments.

3.3 RESULTS AND DISCUSSIONS

3.3.1 Characterization

Due to the importance of 2D materials in catalysis and sensing applications, we have exfoliated the multicomponent quasicrystal line alloys to obtain new 2D structures, which could lead to a new paradigm of a versatile platform for the functionalization of metallic materials and their applications. The cast alloy has been mechanically milled for some time to break the bulk material into smaller particles. Subsequently, the particles were exfoliated in Isopropyl alcohol (IPA) by the pressurized ultrasonication method. The schematic representation of the preparation methodology is shown in Figure 3.1(a). The as-cast material ($Al_{70}Co_{10}Fe_5Ni_{10}Cu_5$) exhibits a decagonal Quasi-crystalline structure, and its crystallographic nature is confirmed by the X-ray diffraction pattern before and after exfoliation, shown in Figure 3.1(b). The indexing of the XRD pattern of the multicomponent bulk and 2D sheets was done as reported by *(Lei et al., 2003)*. However, a small XRD peaks shift was observed due to the presence of other elements like Cu and Fe in the present sample.

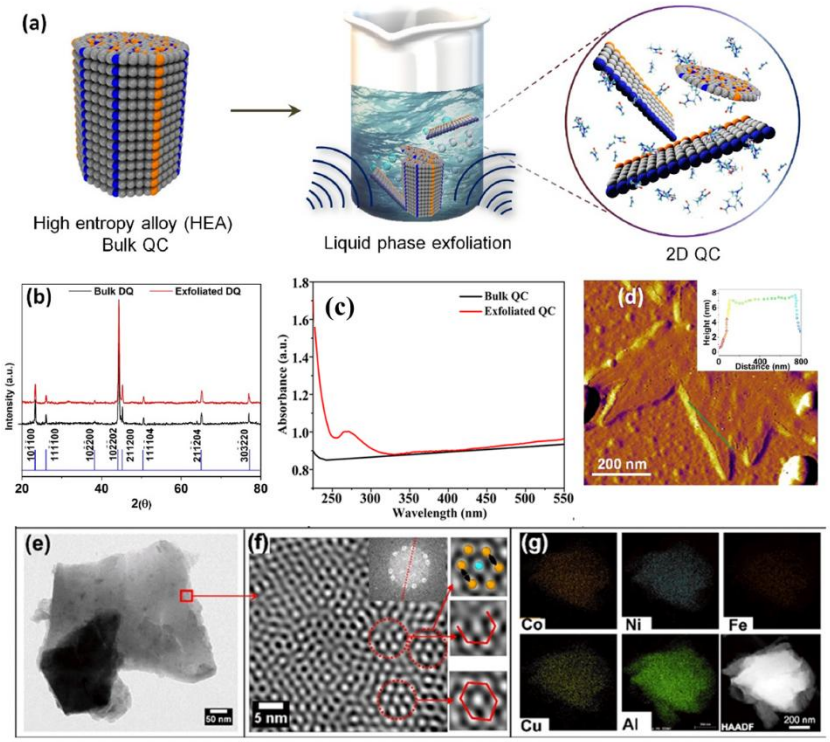

Figure 3.1: (a) Schematic of the preparation and exfoliation methods; (b) XRD patterns of the high entropy alloy (HEA) $Al_{70}Co_{10}Fe_5Ni_{10}Cu_5$ QCs, before and after exfoliation; (c) UV-vis spectra (inset) and the estimated optical band gap by Tauc relation; (d) AFM images of the exfoliated QC and the inset shows the thickness or height variation profile; (e) TEM bright field micrograph of the exfoliated QC; (f) HRTEM image, the inset shows the diffraction pattern; (g) elemental mapping by EDS associated with HRTEM.

The intensity after exfoliation has decreased, possibly due to a reduction in the long-range ordering in the structure. In addition, the surface plasmon resonance (SPR) dominated and provided a strong signal at the nanoscale because of its collective resonance of the conduction electrons and their confinement in the plane. The 2D layers of multicomponent sheets reveal that the SPR signal and peak appeared at λ_{max} ~270 nm, as shown in Figure 3.1(c). The exfoliated wide sheets have a thickness of ~6 nm confirmed by atomic force microscopy, also shown in Figure 3.1(d), and the inset shows the height variation profile. However, the transmission electron microscope (TEM) is endowed with the capability to distinguish unique 2D materials and their planar symmetry. The decagonal 2D quasicrystal has a one-dimensional translational symmetry along the ten-fold rotational axis and other two planar Quasi-periodicities with a two-fold axis . The layered structure of the multicomponent QC ($Al_{70}Co_{10}Fe_5Ni_{10}Cu_5$) can be seen in the bright-field TEM micrograph in Figure 3.1(e) and from the HRTEM image shown in Figure 3.1(f), revealing the decagonal Quasi-crystalline, Quasiperiodic planar symmetry, which corresponds to ten equivalent two-fold symmetry confirmed by SADP (shown in the inset). Other insets in Figure 3.1(f) reveal the quasi-hexagon-like atomic arrangements, which correspond to a 90°-zone axis of ten-fold planar symmetry. Therefore, the exfoliated sheet exhibiting planar atomic arrangement is quasiperiodic in both directions, most suitable for sensing applications. The important characteristic of the multicomponent single-phase QC material is the chemical homogeneity (all elements distributed homogeneously) at the microscopic length scale, which has further been confirmed by the EDS pattern and element mapping associated with the TEM and shown in Figure 3.1(g).

The exfoliated QC dispersion looks like a dark grey solution visually compared to bulk QC due to the exfoliated thin film of QC remaining suspended in the solvent compared to the bulk. The devices have been fabricated using both dispersions (exfoliated and bulk individually) deposited over a printed circuit and dried at 150°C for 20 minutes in an N_2 environment before recording the resistance variation in the presence of different gases (NO_2, NH_3, H_2, H_2S, and SO_2). The gas response was calculated using equation (1).

$$\boldsymbol{Gas\ Response}\ (\%) = \left[\frac{\boldsymbol{R_a - R_g}}{\boldsymbol{R_a}}\right] \times \mathbf{100} \qquad (3.1)$$

where R_{gas} is the resistance during gas exposure, and R_{air} is the resistance under ambient air in the chamber. The exfoliated QC selectivity is higher towards NO_2 gas in comparison to other gases, operating at 100°C, 100 ppm gas concentration. During the sensing, when NO_2 molecules interact with the surface of the sensor, the sudden resistance of the sensor decreases, and under certain conditions, it becomes saturated. The relative response (drop in resistance) by exposure to NO_2 gas in the device is due to the dissociation of the NO_2 molecules, which acts as electron acceptor and modulates the conducting nature of the sensing device (shows p-type nature) and then reaches a steady-state after switching off the gas. The relative gas response of the bulk and exfoliated QC is shown in Figure 3.2(b) and Figure 3.2(c), respectively. The bulk-QC sensor device exhibited a response of 2.25% for 1 ppm NO_2 gas exposure, which increased up to 22% when the gas concentration reached 100 ppm, while the 2D-QC sensor device exhibited a response of 8.85% for 1 ppm NO_2 gas exposure and increased to 46% when the gas concentration reaches 100 ppm Figure 3.2(d). The resistance decreases more with increasing gas concentrations since the gas molecules are expected to dissociate over the device *(L. Yu et al., 2016)*. Adsorption of NO_2 gas on semiconductors increases with increasing temperature in the low-temperature regime, as it is easy to overcome the activation energy barrier *(Rahmani et al., 2009)*. Also, the reaction between adsorbed oxygen and analyte gas becomes easier at higher temperatures, and thus a more significant change in the presence of analyte gas occurs. There is not sufficient energy for NO_2 to be effectively absorbed by gas molecules on the sensor surface at low temperatures *(K. Xu et al., 2021)*. As temperature increases, gas molecule absorption increases on the sensor surface, resulting in an increment in the response. The NO_2 molecules dissociate at very low potentials due to 2D-QC acting as a catalyst. The pseudo bandgap in the lateral direction of the 2D nanosheet

(Dolinšek et al., 2012) plays a crucial role in producing the signal on the ppm level of adsorbate (NO_2 molecules).

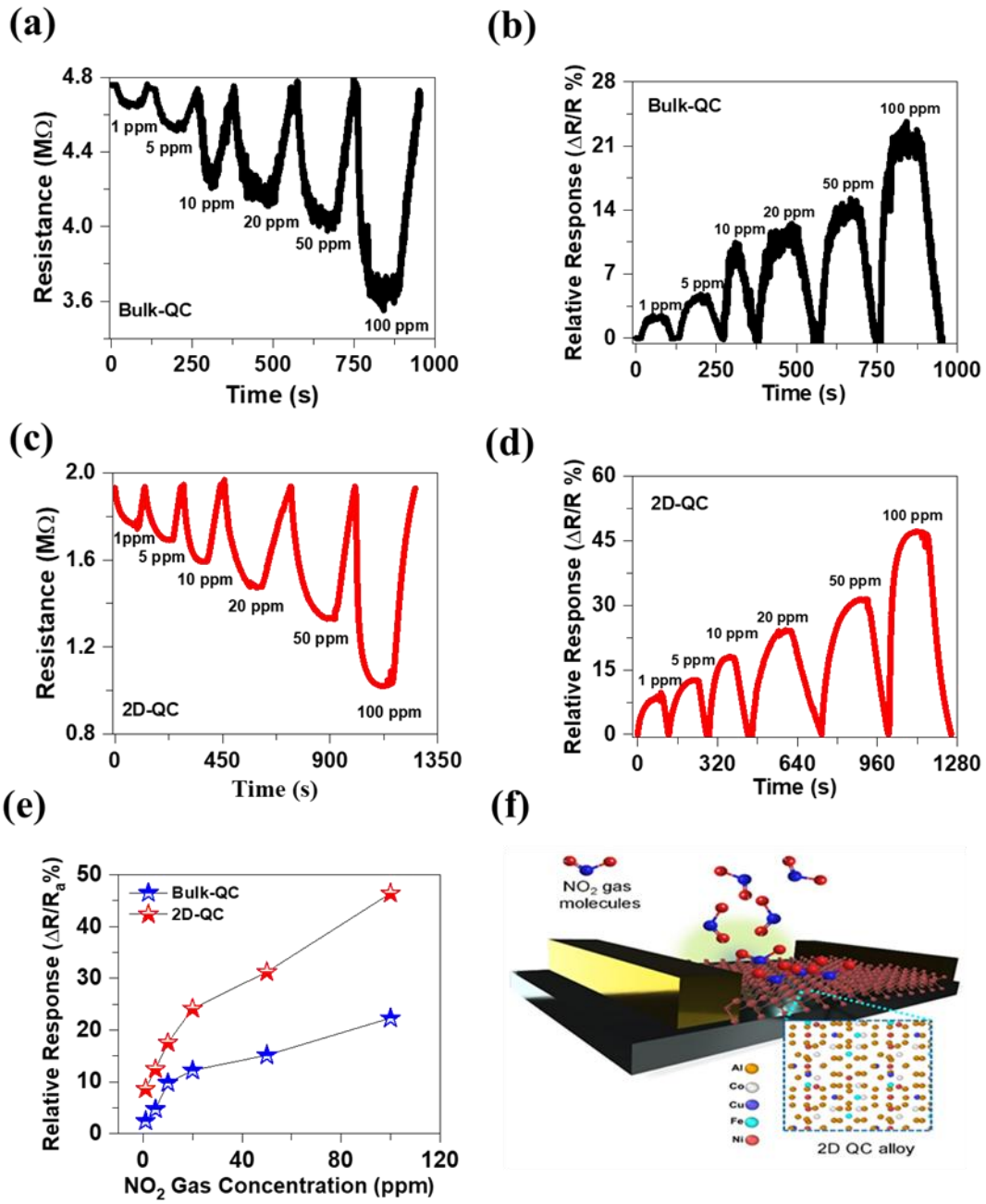

Figure 3.2: (a) Transient resistance curves of the bulk-QC sensor towards 1–100 ppm NO_2 at 100°C, **(b)** Transient relative response curves of the bulk-QC sensor towards 1–100 ppm NO_2 at 100 °C, **(c)** Transient resistance curves of 2D-QC nanosheets sensor towards 1–100 ppm NO_2 at 100°C, **(b)** Transient relative response curves of 2D-QC nanosheets sensor towards 1–100 ppm NO_2 at 100 °C, **(e)** Sensors response curves of bulk-QC and 2D-QC at optimal working temperature 100 °C, **(f)** A schematic of 2D-QC coated over the sensing device and NO_2 molecules landing over the device.

It is to be noted that the operating temperature of the sensor is a crucial factor in reducing energy consumption or operating costs. Therefore, the sensor relative response has been studied at different temperatures by fixing the concentration to 100 ppm NO_2. The sensor's relative response significantly increased from 50°C but got saturated beyond 100 °C, which demonstrated the sensor is working with 100% efficiency at 100 °C, as shown in Figure 3.3(a-b).
The selectivity of the 2D-QC sheet sensor towards NO_2, NH_3, H_2S, H_2, and SO_2 was analyzed, which shows its response to detecting target gases. As shown in Figure 3.3(c), the sensor exhibits

a maximum response (%) of about 46% with the same concentration (100 ppm) NO_2, while the sensitivities to other gases, such as NH_3, H_2S, H_2, and SO_2, are 18%, 9.5%, 6%, and 3.6% respectively. Since synthesized QC shows a slightly p-type nature, the NO_2 (oxidizing gas) sensing resistance decreases, while for other reducing gases resistance of the sensor increases.

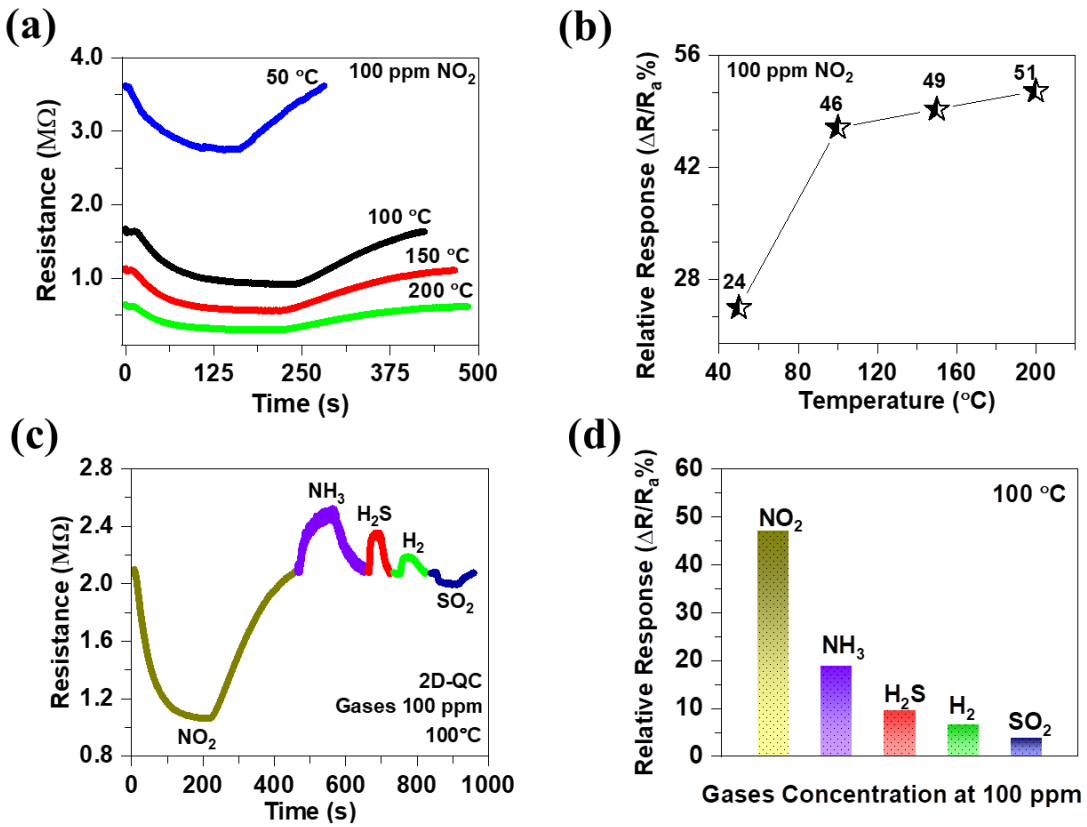

Figure 3.3: (a) Transient resistance curves at different temperatures (50-200 °C) of 2D-QC sensor to 100 ppm concentration of NO_2, **(b)** relative response curve with temperature, (c) Transient resistance curves exposed to 100 ppm of different gases at 100°C, **(d)** A bar graph summarizing the data shown in **(c)**.

To further investigate the relative humidity (RH%) effect at different humidity conditions and get a slight change in resistance under RH% at 100 °C, as shown in Figure 3.4(a) and Figure 3.4(b). At RH 20%, 40%, 60%, and 80%, the base resistance was 2.14 MΩ, 2.04 MΩ, 1.74 MΩ, and 1.63 MΩ, after introducing 100 ppm NO_2 resistance decreases of the sensor with numerical value 1.73 MΩ, 1.68 MΩ, 1.45 MΩ, and 1.35 MΩ respectively, with relative humidity affect 20%, 40%, 60%, and 80%. Under humid conditions, the chemisorption and subsequent dissociation of H_2O molecules on the sensor surface generate surface hydroxyl groups, which act as a barrier to eject an electron from the sensor surface. Hence the response of the sensor decreases with RH%. For suitable sensor repeatability, the baseline resistance under exposure of 10 ppm NO_2 has been repeated cycles to test the feasibility of the sensor. The repeatability results of the 2D-QC sensor are demonstrated in Figure 3.4 (c) and Figure 3.4(d), respectively. It is observed that for each cycle, the variation in sensor resistance is almost the same as 10 ppm of NO_2, which shows good reproducibility of the sensors.

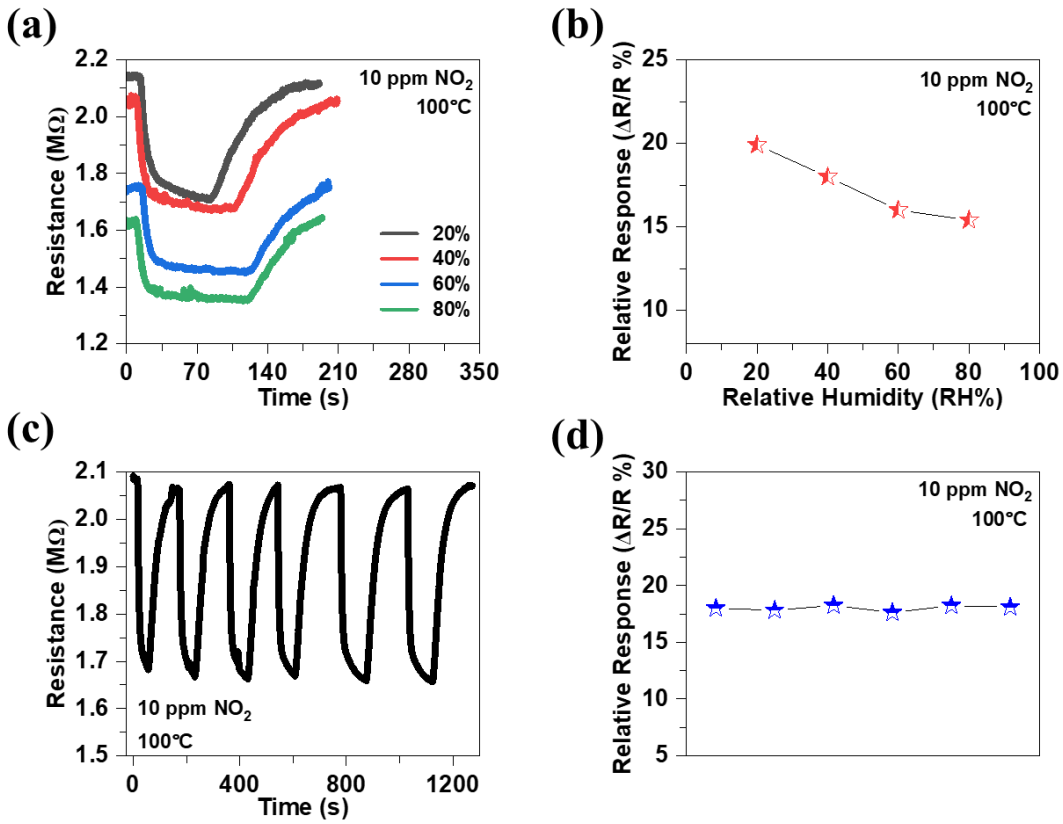

Figure 3.4: (a) Variation in the resistance of the 2D-QC sensor for 10 ppm NO_2 at various humidity levels, **(b)** relative response curve of when sensor device was subjected to 10 ppm NO_2 at RH% summarized the curves shown in **(a), (c)** Short-term repeatability test of 2D-QC sensor towards 10 ppm of NO_2 at 100°C, **(b)** prolonged response curve to summarized **(c).**

Figure 3.5 illustrates the reproducibility of the 2D quasicrystal-based NO_2 sensor tested at 100 °C using three same Parmeter sensor devices: 2D QC-S1, 2D QC-S2, and 2D QC-S3. As shown in **Figure 3.5a**, all three sensors exhibit nearly identical NO_2 response, confirming excellent reproducibility in sensing behavior. **Figure 3.5b** presents the average sensor response along with standard deviation error bars, highlighting minimal variation among the devices. These results demonstrate the robustness and consistency of the fabrication process of the 2D quasicrystal platform for NO_2 sensing applications.

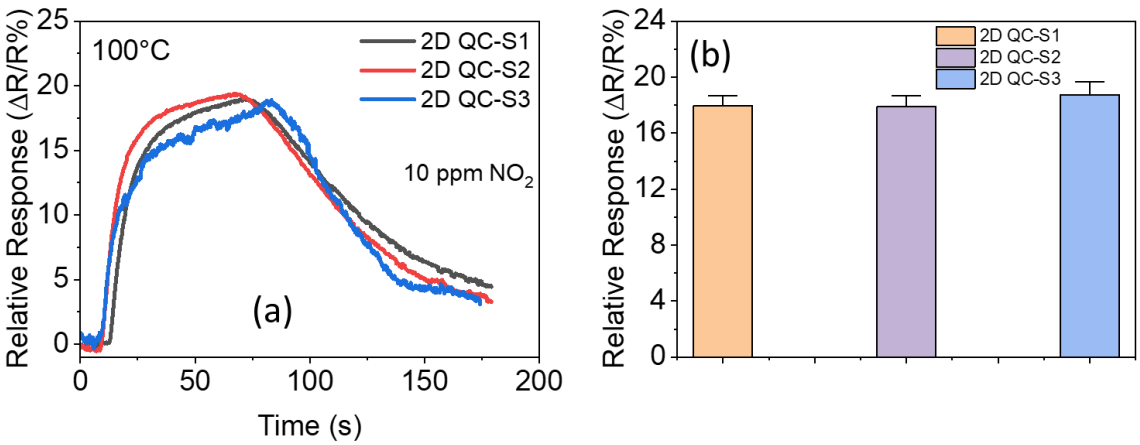

Figure 3.5: reproducibility test on 2D quasicrystal sensor at a temperature 100°C after making three devices namely sensor 2D QC-S1, 2D QC-S2, 2D QC-S3 with the same parameters (b) error bars displaying the average and standard deviation of the performance of sensors.

3.4 GAS SENSING MECHANISM

The 2D-$Al_{70}Co_{10}Fe_5Ni_{10}Cu_5$ dispersion was coated over the device and dried in an open environment. Therefore, the adsorption of oxygen molecules on the surface of the 2D thin film is obvious. Thus, the oxygen molecule's action is considered in two ways during sensing, such as oxygen molecules remaining physically adsorbed on the QC surface or oxygen molecules gaining an electron because of the oxidizing behavior. The adsorbed oxygen molecules are attracted toward electrons, the reaction process can be written as shown in equations (3.2) to (3.3).

$$O_2(gas) \leftrightarrow O_{2(ads)} \quad (3.2)$$
$$O_{2(ads)} + e^- \leftrightarrow O_{2^-(ads)} \quad (3.3)$$

As NO_2 is exposed to the QC surface, electrons will be transferred from QC to the NO_2 gas molecules, and as a result, the hole concentrations increased of the sensing surface layer as per equation (3.4).

$$NO_2\ (gas) + e^- \leftrightarrow NO_{2^-(ads)} \quad (3.4)$$

Such as, bulk and 2D Quasicrystal $Al_{70}Co_{10}Fe_5Ni_{10}Cu_5$ work as a sensor, and the sensor device mechanism is based on the change in resistance due to the air oxygen molecule's chemisorption on the sensing surface. Initially, when the $Al_{70}Co_{10}Fe_5Ni_{10}Cu_5$ sensor surface is in the air, the air oxygen molecules in the form of O_2- adsorb on the sensor surface. Then the sensor resistance decreased due to the formation of a very thick space charge layer of electrons on the surface. As we are exposing the NO_2 (electron-accepting) gas which has a large electron affinity compared to O_2, the tendency to take electrons is high compared to O_2 *(Ou et al., 2015)*. Hence NO_2 is responsible for a significant change in the resistance. To corroborate the absorption or sensing theory, the interaction of the 2D-QC sheet with the NO_2 molecules and charge density region for NO_2 and H_2 have been deduced using density functional theory (DFT) simulations.

To obtain insights to understand and interpret the experimental observations, we performed *ab initio* density functional theory (DFT) simulations at the local density approximation (LDA) level as implemented in the SIESTA code *(Soler et al., 2002b)*. Our DFT picture is based on the numerical localized atomic orbitals to represent the wave function using a double-ζ basis set with polarized functions (DZP) as a linear combination of atomic orbitals. To include the interaction between valence electrons and core ions, we used the norm-conserving Troullier Martins ultrasoft pseudopotential *(Troullier et al., 1991)*. Some values for energy mesh cut-off have been tested and validated that the value of 250 Ry can be used to describe the charge density in real space with high accuracy. All calculations were made at gamma point to represent the special k-point grid because we considered the structural models as finite systems that can be treated as a large-molecules (the lack of symmetry precludes the use of cyclic boundary conditions (crystals)). The convergence criteria for the density matrix are considered satisfied when the difference between the input and output of a self-consistent field value is smaller than 10^{-6} eV.

The optimized QC crystal layer structure is a rectangle with lattice vectors of 18.2 and 18.8 Å along X and Y, respectively. Furthermore, to prevent spurious interactions between QC layers and/or the deposited molecules with its periodic images, we used a vacuum buffer layer of 30 Å along the Z direction.

To calculate the interaction between the QC layer and NO_2 and H_2 molecules, we randomly distributed each molecule on the whole QC, and the adsorption energy for each equilibrium configuration is calculated by the expression:

$$E_{ad} = ((E_{(QC+mol)} - E_{QC} - E_{mol})/N) \quad (3.5)$$

Where *N* is the total number of atoms, E_{QC+mol} is the total energy for QC plus molecule, $E_{QC,}$ and E_{mol}, are the total energy for isolated QC and molecule, respectively.

The equilibrium geometries were obtained at T = 0K from DFT and at T=373K from *ab initio* molecular dynamics simulations corresponding to the same temperature regime investigated in

the experiment. We have also analyzed the electrical transport properties considering a non-equilibrium Green function formalism and using the TRANSIESTA code, where the non-equilibrium green function formalism is implemented. We have considered that QC plus molecule region in contact with a left and right gold electrode for an infinite system in the transport direction. In this case, a dense mesh 1x1x60 cut off k-points along the transport direction. A finite applied voltage V is defined by the difference of the chemical potentials at the electrodes and the transmission coefficients can be obtained and related to the current value I. We present the IV plots for the most stable NO_2 and H_2 molecule configurations. Figure 3.5(a) shows the QC crystal layer structure interacting with the NO_2 molecule corresponding to a particular equilibrium geometry at T = 0 K. As per the assumption of the initial condition, the molecule is placed above the QC for different molecular configurations where the molecule is placed at different positions of QC, and the system is set free to evolve mimicking the scanning of the best energy configurations. It was observed that, even for T= 0 K, the NO_2 (and H_2) molecule. In the majority of cases tends to dissociate, consistent with the experimental observations and attributed to the QC catalytic effects. This effect is also observed for more layers of QC, for instance, for two and three layers. When temperature effects are considered from *ab initio* molecular dynamics at T = 373 K, the reaction facilitates molecular dissociation due to the entropic effects caused by thermal fluctuations. To estimate the adsorption energy values, we considered only configurations where molecules remain intact and do not dissociate and we found that the adsorption energy values are very similar for different parts of QC. For, both NO_2 and H_2 molecules, the tendency is similar to the one observed in Figure 3.5(a), in which the molecules are aligned to the QC plane, and the most stable configuration occurs close to the Fe-Ni-Cu atoms. The adsorption energy values for NO_2 range between -289 and - 233 meV/atom, while the values for H_2 are between -17 and -4 meV/atom. This agrees with experimental observations, where NO_2 exhibits a stronger response than other molecules.

The experimental measurements suggest that NO_2 is an electron acceptor due to the large electron affinity compared to other molecules. The spatial charge distribution has been calculated for the most stable configuration of NO_2 and H_2 molecules, shown in Figure 3.5(b) to obtain some insight into this experimental observation. It is clearly stated that there is an appreciated electron density around the NO_2 molecule in Figure 3.5(b). In contrast, the electron density around the H_2 molecule in Figure 3.5(c) is practically null. Thus, we have strong evidence that chemisorption occurs for the NO_2 molecule deposited at the QC crystal structure. For the configuration shown in Figure 3.5(b), the Nitrogen is closer to the iron atom (distance of 1.93 Å), whereas the two oxygens are at 1.99 and 2.13 Å from the Ni atoms. These values are in agreement with the literature, where the typical reported values are 2.11 and 2.05 Å for Fe-N and Ni-O bonds, respectively. Finally, the I-V characteristic as shown in Figure 3.5(d), is the most stable configuration of NO_2 and H_2. As observed in the experimental section, here we see clearly that current (I) tends to be greater for NO_2 in comparison to H_2 molecule, which is consistent with experimental where the sign of sensor is more significant for the NO_2 case.

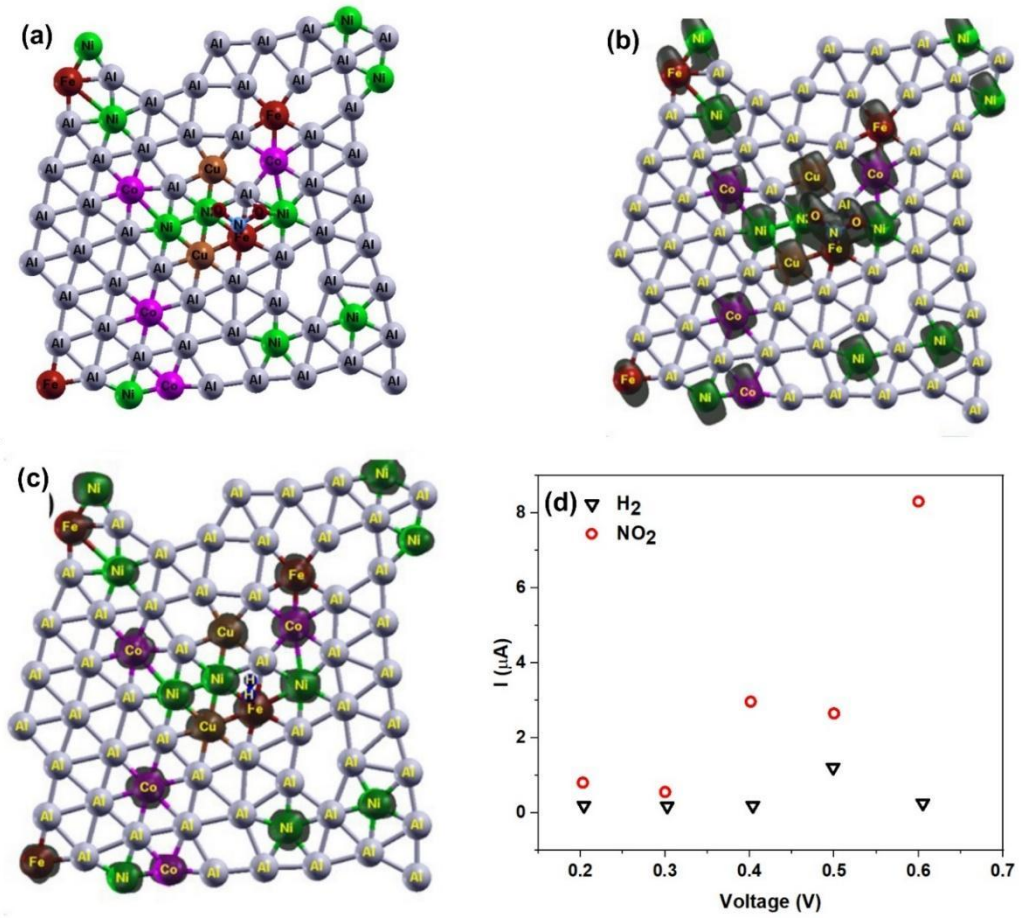

Figure 3.6: (a) One equilibrium geometry for NO_2 molecule adsorbate on the QC crystal; spatial distribution of the charge density in QC for geometry equilibrium corresponding to the most stable configuration for NO_2; **(b)** H_2 **(c); (d)** Current I versus the applied voltage V for the most stable configuration of NO_2 (black balls) and H_2 (red balls).

When exposed to NO_2 and adsorbed on the sensor surface, part of the conduction band electrons are extracted from the 2D-QC and captured by NO_2^-, which is chemisorbed on the surface of the sensing material. At lower temperatures, the NO_2^- is dominant. This chemisorption also increases the hole concentration in the valence band, which increases the electrical conductivity, i.e., resistance decreases. For a reducing gas, the opposite phenomenon occurs. It reacts with absorbed oxygen species (O_2^-, O^-) and releases electrons, which go back into the conduction band of the material, and the resistance of the sensor increases. In the NO case, the oxidation state of N is +2, and by losing electrons, it can go to higher oxidation states and act as a reducing agent. Thus, during the NO sensing, the resistance of the sensor will increase. Nitrous oxide (N_2O) is a strong oxidizing agent; hence same as NO_2 sensing, the resistance of N_2O sensor resistance will decrease. The device response and recovery time increase with temperature in part because there is a probability that QC crystal can oxidize with increasing temperatures. A more sensitive response is expected at low concentrations since increased concentrations increase the surface coverage, thus increasing the repulsion of the neighboring adsorbed NO_2 molecules, which increases the slope of ($\Delta R/R$) vs. NO_2 concentration curve.

Table 3.1: Working temperature comparison of other NO_2 gas sensors.

Composition /Materials	Synthesis method	Sensing Temp. (°C)	NO_2 Conc.	Gas Response	Reference
$Na_{0.51}Bi_{0.50}TiO_3-\delta\delta$	Sol-Gel	400-600	500 ppm	11.23 µA*	*(Y. Xiao et al., 2017)*
2D MoS_2	CVD	100	20 ppm	120% **	*(B. Cho et al., 2015)*
5,10,15,20-tetrakis (4-(2,4 diaminotriazinyl)-phenyl)porphyrin(H2 TDPP)	Solvothermal	RT	2000 ppb	43.3%***	*(Y. Wang, Liu, et al., 2020)*
2D-NbS_2	CVD	RT	5 ppm	15%***	*(Y. Kim et al., 2019)*
$Gd_{2-\delta x}M_xZr_2O7+\delta$	Hydrothermal	500	500 ppm	2.42 µA*	*(Zhong et al., 2017)*
2D-quasicrystal ($Al_{70}Co_{10}Fe_5Ni_{10}Cu_5$)	Chemical exfoliated method	100	100 ppm	46%***	*This work*

* ($\Delta I = I_g - I_a$), ** (R_a/R_g%), *** (($\Delta R = (R_a - R_g)/R_a$%))

3.5 Chapter Summary

In this chapter, the exfoliation of multicomponent metallic alloy into 2D-sheets and their use in NO_2 gas sensing is based on a resistive mechanism. The obtained exfoliated structures have an average thickness and lateral dimension of around 6 nm with a micron size width, which were estimated from extensive TEM analyses and are consistent with previous related work *(S. S. Mishra et al., 2022)*. These structures significantly enhanced the sensitivity of the sensor as well as its selectivity. The stable multi-element metallic alloys with single-phase offer higher selectivity due to the predominately many active sites distributed homogeneously over the material surface. The sensing mechanism is based on the change in the resistivity of the material. The demonstrated device is highly selective towards the NO_2 gas compared to other gases (NH_3, H_2S, H_2, SO_2, etc.). Density functional theory simulations further corroborate that the NO_2 molecules are highly prone to be adsorbed on the 2D $Al_{70}Co_{10}Fe_5Ni_{10}Cu_5$ sheets and adsorbed oxygen molecules at the surface play a significant role in the sensitive detection. The chemical composition of the exfoliated quasicrystal sheets was determined by using EDS analysis and HRTEM EDS mapping *(S. S. Mishra et al., 2022)*. This work significantly extends the use of metal-based smart sensing materials and further develops their potential environment monitoring applications.